A farnesyltransferase inhibitor improves disease phenotypes in mice with a Hutchinson-Gilford progeria syndrome mutation

Shao H. Yang,[1] Margarita Meta,[2] Xin Qiao,[1] David Frost,[3] Joy Bauch,[3] Catherine Coffinier,[1] Sharmila Majumdar,[2] Martin O. Bergo,[4] Stephen G. Young,[1] and Loren G. Fong[1]

[1]Department of Medicine, Division of Cardiology, David Geffen School of Medicine, UCLA, Los Angeles, California, USA. [2]Department of Radiology, UCSF, San Francisco, California, USA. [3]Abbott, Abbott Park, Illinois, USA. [4]Department of Medicine, Wallenberg Laboratory, Sahlgrenska University Hospital, Göteborg, Sweden.

Hutchinson-Gilford progeria syndrome (HGPS) is caused by the production of a truncated prelamin A, called progerin, which is farnesylated at its carboxyl terminus. Progerin is targeted to the nuclear envelope and causes misshapen nuclei. Protein farnesyltransferase inhibitors (FTI) mislocalize progerin away from the nuclear envelope and reduce the frequency of misshapen nuclei. To determine whether an FTI would ameliorate disease phenotypes in vivo, we created gene-targeted mice with an HGPS mutation ($Lmna^{HG/+}$) and then examined the effect of an FTI on disease phenotypes. $Lmna^{HG/+}$ mice exhibited phenotypes similar to those in human HGPS patients, including retarded growth, reduced amounts of adipose tissue, micrognathia, osteoporosis, and osteolytic lesions in bone. Osteolytic lesions in the ribs led to spontaneous bone fractures. Treatment with an FTI increased adipose tissue mass, improved body weight curves, reduced the number of rib fractures, and improved bone mineralization and bone cortical thickness. These studies suggest that FTIs could be useful for treating humans with HGPS.

Introduction

Hutchinson-Gilford progeria syndrome (HGPS) is a rare pediatric progeroid syndrome characterized by multiple disease phenotypes, including slow growth, sclerodermatous changes of the skin, alopecia, micrognathia, osteoporosis, osteolytic lesions in bone, and occlusive atherosclerotic vascular disease (1–5). HGPS is caused by an *LMNA* mutation that results in the synthesis of a mutant prelamin A, commonly called progerin, that contains a 50-amino-acid deletion within the carboxyterminal portion of the protein (2, 6). Progerin undergoes farnesylation at a carboxyterminal CaaX motif, but it lacks the cleavage site for the endoprotease ZMPSTE24 and therefore cannot be further processed to mature lamin A (2, 6). Within cells, progerin is targeted to the nuclear envelope, where it interferes with the integrity of the nuclear lamina and causes misshapen nuclei (7–9).

We suspected that protein farnesylation might be crucial for the targeting of progerin to the nuclear rim, and we hypothesized that blocking farnesylation with a farnesyltransferase inhibitor (FTI) would mislocalize progerin away from the nuclear rim and reduce the frequency of misshapen nuclei (6, 9, 10). Indeed, this was the case; an FTI reduced the number of misshapen nuclei in fibroblasts from mice with a targeted HGPS mutation (9). Subsequently, we (10) and others (11–13) showed that FTIs also improved nuclear shape in fibroblasts from humans with HGPS.

The fact that FTIs improved nuclear shape in HGPS cells raised hope for a potential therapy and stimulated interest in testing the efficacy of FTIs in a gene-targeted mouse model of HGPS (6, 9–13). In this study, we describe disease phenotypes in mice carrying a targeted HGPS mutation and define the impact of FTI treatment on the course of the disease.

Results

Slow growth, bone abnormalities, and loss of fat in $Lmna^{HG/+}$ mice. The tissues of $Lmna^{HG/+}$ mice (mice heterozygous for a targeted HGPS mutation [ref. 9] yielding exclusively progerin) expressed lamin A, lamin C, and progerin. The amount of progerin in both liver and aorta was greater than that of lamin A or lamin C, as judged by Western blotting (Figure 1A). Homozygous mice ($Lmna^{HG/HG}$) expressed exclusively progerin (Figure 1A).

$Lmna^{HG/+}$ mice appeared normal for the first 3 weeks of life. By 6–8 weeks, however, both male and female $Lmna^{HG/+}$ mice began to lose weight (Figure 1B). The survival of $Lmna^{HG/+}$ mice was reduced (Figure 1C). Also, $Lmna^{HG/+}$ mice had significantly less subcutaneous fat and abdominal fat (Figure 1, D and E) and exhibited more kyphosis of the spine (Figure 2, A and B). $Lmna^{HG/+}$ mice invariably developed osteolytic lesions in the ribs, predisposing to rib fractures near the costovertebral junction (Figure 2, C and D). By 18 weeks of age, all $Lmna^{HG/+}$ mice (n = 11 examined) developed osteolytic lesions in the posterior portion of the zygomatic arch (Figures 2, E and F); they also had micrognathia and a reduction in the zigzag appearance of the cranial sutures (Figure 2, E and F). Some $Lmna^{HG/+}$ mice had osteolytic lesions in other sites (e.g., clavicle, scapula, calvarium, and mandible). The $Lmna^{HG/+}$ mice became progressively malnourished, and 50% (39/78) died or were so sick that they had to be euthanized by 27 weeks of age.

Nonstandard abbreviations used: FTI, farnesyltransferase inhibitor; HGPS, Hutchinson-Gilford progeria syndrome.

Conflict of interest: The authors have declared that no conflict of interest exists.

Citation for this article: *J. Clin. Invest.* **116**:2115–2121 (2006). doi:10.1172/JCI28968.

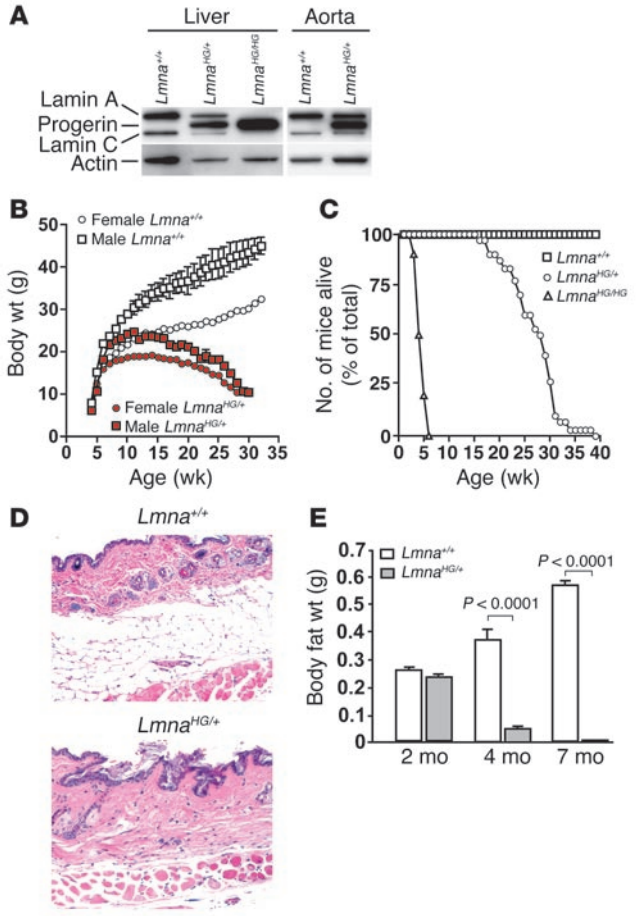

Figure 1
Phenotypes of *Lmna*$^{HG/+}$ mice. (**A**) Western blot (with an antibody against lamin A/C), revealing progerin, lamin A, and lamin C in the liver and aorta of *Lmna*$^{HG/+}$ mice and progerin in the liver of *Lmna*$^{HG/HG}$ mice. (**B**) Retarded growth in male and female *Lmna*$^{HG/+}$ mice. Body weight curves are shown for male *Lmna*$^{HG/+}$ mice (n = 8) and littermate male *Lmna*$^{+/+}$ mice (n = 6) and for female *Lmna*$^{HG/+}$ mice (n = 8) and littermate female *Lmna*$^{+/+}$ mice (n = 7). Error bars for female mice and male *Lmna*$^{HG/+}$ mice are too small to be seen. (**C**) Reduced survival of *Lmna*$^{HG/+}$ (n = 42) and *Lmna*$^{HG/HG}$ (n = 12) mice. (**D**) Representative H&E-stained sections of skin from a 6-month-old *Lmna*$^{HG/+}$ mouse and a littermate *Lmna*$^{+/+}$ mouse; n = 4 mice of each genotype examined. (**E**) Body fat in *Lmna*$^{HG/+}$ (n = 4) versus *Lmna*$^{+/+}$ mice (n = 3) at 2 months of age (P = 0.2); *Lmna*$^{HG/+}$ (n = 8) versus *Lmna*$^{+/+}$ mice (n = 8) at 4 months of age (P < 0.0001); and *Lmna*$^{HG/+}$ (n = 5) versus *Lmna*$^{+/+}$ mice (n = 6) at 7 months of age (P < 0.0001). Original magnification, ×20.

Many of the phenotypes in *Lmna*$^{HG/+}$ mice (e.g., slow growth, weight loss, loss of adipose tissue, kyphosis, osteolytic lesions in the zygomatic arch, and fractured ribs at the costovertebral junction) are shared by *Zmpste24*$^{-/-}$ mice (14, 15). However, one difference was noteworthy: *Zmpste24*$^{-/-}$ mice developed a grip strength abnormality (inability to hang upside down from a grid at 4 months of age) (14, 15), whereas in *Lmna*$^{HG/+}$ mice the grip strength was invariably normal (Figure 2G). No histological abnormalities in skeletal muscle were identified in *Lmna*$^{HG/+}$ mice. The aortas of 6- to 7-month-old mice (n = 8) were also examined by routine histology; the intima, media, and adventitia of *Lmna*$^{HG/+}$ aortas were normal, free of lesions, and indistinguishable from those of *Lmna*$^{+/+}$ (wild-type) mice (Figure 2H).

Early death and severe bone abnormalities in Lmna$^{HG/HG}$ *mice.* In sustained breeding efforts, we were able to obtain only a few (n = 12) homozygous mice (*Lmna*$^{HG/HG}$). *Lmna*$^{HG/HG}$ mice were invariably very small (approximately one-half the size of their littermates), with a complete absence of adipose tissue, and many had spontaneous bone fractures in the extremities (Figure 3, A and B). All *Lmna*$^{HG/HG}$ mice died by 3–4 weeks of age (Figure 1C). As judged by μCT scans, the bones of *Lmna*$^{HG/HG}$ mice were poorly mineralized; the mice also had micrognathia and an abnormal skull shape, with open cranial sutures (Figure 3, C–F).

We suspected that the more severe disease phenotypes in *Lmna*$^{HG/HG}$ mice would be accompanied by more extensive abnormalities in nuclear shape in cultured cells. Indeed, a high frequency of nuclei from *Lmna*$^{HG/HG}$ fibroblasts were misshapen (59.5% of nuclei had folds or blebs versus 29.6% in *Lmna*$^{HG/+}$ cells and 10.8% in *Lmna*$^{+/+}$ cells; more than 1,000 cells counted for 2 different fibroblast cell lines of each genotype; P < 0.0001 by χ^2 test) (Figure 4). Treatment of *Lmna*$^{HG/+}$ and *Lmna*$^{HG/HG}$ fibroblasts with an FTI significantly reduced the frequency of misshapen nuclei (P < 0.0001).

The phenotype of *Lmna*$^{HG/-}$ mice (mice with 1 *Lmna*^{HG} allele and 1 *Lmna*-knockout allele; ref. 16) was less severe than that of *Lmna*$^{HG/HG}$ mice but more severe than that of *Lmna*$^{HG/+}$ mice. *Lmna*$^{HG/-}$ mice (n = 10) had multiple rib fractures by 8 weeks of age (resembling 5- to 6-month-old *Lmna*$^{HG/+}$ mice), and all *Lmna*$^{HG/-}$ mice died by 10–14 weeks of age (data not shown).

Amelioration of disease phenotypes in Lmna$^{HG/+}$ *mice with an FTI.* To determine whether an FTI would improve disease phenotypes in *Lmna*$^{HG/+}$ mice, we administered a potent FTI, ABT-100 (17), in the drinking water (39 mg/kg body weight) to groups of 7–10 male and female *Lmna*$^{HG/+}$ mice and 6–9 male and female littermate *Lmna*$^{+/+}$ mice, beginning at 4 weeks of age. Biomarker studies indicated that the FTI was active in vivo. First, the FTI interfered with the biogenesis of mature lamin A from the wild-type (*Lmna*$^{+}$) allele, resulting in the appearance of nonfarnesylated prelamin A in the livers of FTI-treated mice, which could be readily detected by Western blotting with a prelamin A–specific antibody (Figure 5A). Second, Western blots of HDJ-2, a chaperone protein that is normally farnesylated, revealed that approximately 70–80% of the HDJ-2 in the livers of FTI-treated mice was nonfarnesylated (Figure 5A).

In *Lmna*$^{+/+}$ female mice, the FTI reduced body weight compared with *Lmna*$^{+/+}$ mice given the vehicle alone (P = 0.03) (Figure 5B); however, the FTI had no apparent effect on weight gain in male *Lmna*$^{+/+}$ mice (Figure 5C). Aside from the minor changes in body weight in the female mice, the FTI had no noticeable side effects. In contrast, the FTI improved body weight curves in both female and male *Lmna*$^{HG/+}$ mice (P < 0.0001) (Figure 5, B and C). FTI treatment increased the weight of the major fat pads in *Lmna*$^{HG/+}$ mice (P = 0.002) (Figure 5D) and also increased the amount of fat in subcutaneous tissues (Figure 5E).

The FTI treatment significantly improved, but did not completely cure, the bone disease in *Lmna*$^{HG/+}$ mice. The degree of kyphosis was reduced in FTI-treated *Lmna*$^{HG/+}$ mice (kyphotic index: 3.32 ± 0.37 in FTI-treated *Lmna*$^{HG/+}$ mice versus 1.91 ± 0.38 in vehicle-treated littermate *Lmna*$^{HG/+}$ mice; P = 0.02) (Figure 6, A and B). The FTI-treated mice also developed fewer rib fractures (1.13 ± 1.45 in FTI-treated *Lmna*$^{HG/+}$ mice versus 9.1 ± 3.76 in vehicle-treated littermate *Lmna*$^{HG/+}$ mice; P < 0.0001) (Figure 6C). The reduced number of rib

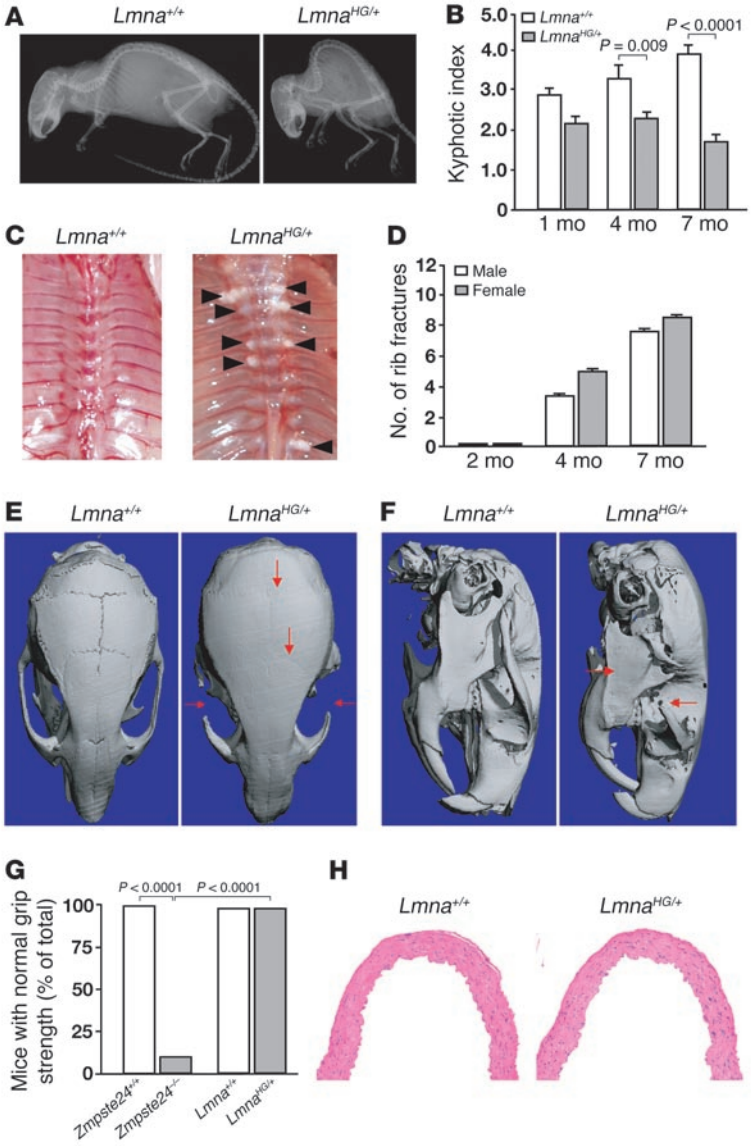

Figure 2
Phenotypes in *Lmna*$^{HG/+}$ mice. (**A**) Radiograph of a 6-month-old *Lmna*$^{HG/+}$ mouse and a littermate *Lmna*$^{+/+}$ mouse. (**B**) Kyphotic index of *Lmna*$^{HG/+}$ and *Lmna*$^{+/+}$ mice at 1 month ($P = 0.076$), 4 months ($P = 0.009$), and 7 months ($P < 0.0001$) of age ($n = 4$ per group). (**C**) Thorax of a 6-month-old *Lmna*$^{HG/+}$ mouse and a littermate *Lmna*$^{+/+}$ mouse. Black arrowheads indicate fracture callus surrounding broken ribs. (**D**) Number of rib fractures in 2-month-old *Lmna*$^{HG/+}$ female ($n = 3$) and male ($n = 4$) mice, 4-month-old *Lmna*$^{HG/+}$ female ($n = 10$) and male ($n = 8$) mice, and 7-month-old *Lmna*$^{HG/+}$ female ($n = 7$) and male ($n = 7$) mice. No rib fractures were observed in *Lmna*$^{+/+}$ mice. (**E**) Surface renderings of μCT scans of the skulls of 4-month-old *Lmna*$^{HG/+}$ and *Lmna*$^{+/+}$ mice. Red arrows indicate a characteristic absence of the zigzag appearance of the cranial sutures and osteolytic lesions of the zygomatic arch. (**F**) Surface renderings of μCT scans of the skulls of 4-month-old *Lmna*$^{HG/+}$ and *Lmna*$^{+/+}$ mice. Red arrows in the *Lmna*$^{HG/+}$ skull indicate micrognathia and the site of an osteolytic lesion of the zygomatic arch. (**G**) Percentage of 4.5-month-old *Zmpste24*$^{-/-}$ ($n = 16$), littermate *Zmpste24*$^{+/+}$ ($n = 11$), *Lmna*$^{HG/+}$ ($n = 30$), and littermate *Lmna*$^{+/+}$ mice ($n = 12$) with normal grip strength (ability to hang upside down from a grid for 60 seconds). $P < 0.0001$ for both *Zmpste24*$^{-/-}$ versus *Zmpste24*$^{+/+}$ mice and *Zmpste24*$^{-/-}$ versus *Lmna*$^{HG/+}$ mice. (**H**) H&E-stained sections of the ascending aorta from a 7-month-old *Lmna*$^{HG/+}$ mouse and a littermate *Lmna*$^{+/+}$ mouse. Original magnification, ×20.

fractures was evident on μCT scans (Figure 6D). FTI treatment of *Lmna*$^{HG/+}$ mice also led to an improvement in bone mineralization and cortical thickness (Figure 6, E and F).

Discussion

Our first goal was to define the phenotype of gene-targeted mice expressing progerin, the mutant protein responsible for HGPS. The *Lmna*$^{HG/+}$ mice were normal at birth but then exhibited many of the hallmarks that appear early on in humans with HGPS, such as slow growth, osteolytic lesions in bone, osteoporosis, micrognathia, and loss of adipose tissue. These phenotypes were even more dramatic in *Lmna*$^{HG/HG}$ mice. A second goal was to determine whether treatment with an FTI would ameliorate disease phenotypes in *Lmna*$^{HG/+}$ mice. Our studies provided a clear answer: an FTI, administered at 4 weeks of age, improved body weight curves, prevented loss of adipose tissue, improved bone mineralization, and reduced the number of rib fractures. Very recently, Fong et al. (18) reported that an FTI ameliorated disease phenotypes in *Zmpste24*$^{-/-}$ mice. An absence of ZMPSTE24, the prelamin A endoprotease, leads to an accumulation of wild-type prelamin A — not the progerin molecule found in humans with HGPS. The current studies with a mouse HGPS model showed that an FTI ameliorates disease phenotypes caused by progerin, providing support for the notion that FTIs could be useful for treating human HGPS patients.

The phenotypes in *Lmna*$^{HG/+}$ mice closely resemble those in *Zmpste24*$^{-/-}$ mice. These phenotypic similarities were reassuring, given that both mouse models have an accumulation of one form of farnesyl–prelamin A (a wild-type prelamin A in *Zmpste24* deficiency and the truncated prelamin A in HGPS). However, one phenotypic difference was clear: unlike the *Zmpste24*$^{-/-}$ mice, *Lmna*$^{HG/+}$ mice did not develop a grip strength abnormality. The absence of the grip abnormality in *Lmna*$^{HG/+}$ mice underscores that these mice constitute a faithful model of human HGPS, since children with HGPS do not exhibit significant muscle weakness (1). It is not clear why the *Zmpste24*$^{-/-}$ mice had muscle weakness, whereas the *Lmna*$^{HG/+}$ mice did not. Clearly, the *Zmpste24*$^{-/-}$ mice are sicker mice, in general, than the *Lmna*$^{HG/+}$ mice, but that may not be the entire explanation, since *Lmna*$^{HG/+}$ mice retained normal grip strength even when they were very debilitated.

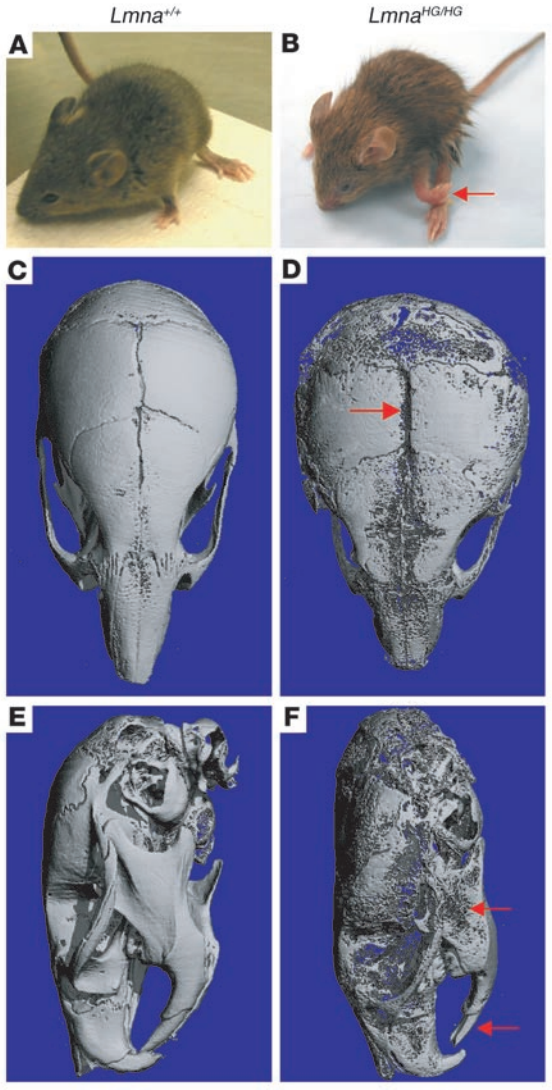

Figure 3
Lmna$^{HG/HG}$ mice are small and have poorly mineralized bone. (**A** and **B**) Photographs of 17-day-old *Lmna*$^{+/+}$ (**A**) and *Lmna*$^{HG/HG}$ (**B**) mice. The *Lmna*$^{HG/HG}$ mouse had a spontaneous fracture in the left forelimb (red arrow). (**C**–**F**) Surface renderings of μCT scans of the skull (performed at exactly the same threshold) for a 17-day-old *Lmna*$^{HG/HG}$ mouse (**D** and **F**) and littermate *Lmna*$^{+/+}$ mouse (**C** and **E**). (**C** and **D**) Top view of skulls. The *Lmna*$^{HG/HG}$ skull is misshapen, poorly mineralized, and exhibits incomplete fusion of the cranial sutures (red arrow). (**E** and **F**) Lateral view of skulls. The *Lmna*$^{HG/HG}$ skull is misshapen, with a small mandible (upper red arrow) and a short lower incisor (lower red arrow).

The expression of severe disease phenotypes in mice heterozygous for the *Lmna*^{HG} allele underscores the potency of progerin in eliciting disease phenotypes. Other groups had previously used gene targeting to create mice with a *Lmna*-knockout mutation (16) and various *Lmna* missense mutations (19–21). In those cases, homozygous mice had distinct phenotypes, whereas the heterozygous mice were indistinguishable from wild-type mice.

Occlusive disease of the large arteries is a late phenotype of humans with HGPS, apparent during the second decade of life and often leading to fatal stroke or myocardial infarction. The mechanisms underlying the occlusive arterial disease are uncertain. Pathologic studies of several progeria patients by Stehbens and coworkers (4, 5) and Ackerman and Gilbert-Barness (3) revealed moderately severe atherosclerotic lesions in the arterial intima along with the loss of some smooth muscle cells in the arterial media. The *Lmna*$^{HG/+}$ mice did not have histopathological abnormalities in the intima or media of the aorta, even though they clearly exhibited many of the early hallmarks of HGPS. We do not know why the *Lmna*$^{HG/+}$ mice did not develop disease in their large arteries, but we suspect that they simply did not live long enough for this late HGPS phenotype to emerge. Recently, Varga et al. (22) created transgenic mice with a 164-kb human bacterial artificial chromosome spanning 4 genes — *RAB25*, *UBQLN4*, *MAPBPIP*, and *LMNA* (engineered to contain the G608G HGPS mutation; ref. 2). The amount of progerin expressed in the tissues of transgenic mice, relative to the amounts of human and mouse lamin A and lamin C, was not clear. The transgenic mice did not manifest any of the early hallmarks of progeria, nor did they have arterial intimal lesions or vascular occlusions, but they did exhibit loss of smooth muscle cells in the media of the aorta (22). The explanation for this constellation of findings is not clear.

In this study, an FTI ameliorated disease phenotypes in *Lmna*$^{HG/+}$ mice but fell short of curing the disease. The concentration of the FTI in the plasma of mice in these studies was low relative to that achieved in earlier anticancer studies (17); in the future, it will be interesting to determine whether a higher dose of an FTI would be more efficacious in preventing disease. Also, it will be important to test the efficacy of an FTI in reversing disease phenotypes in mice after they are well established, as the ability to *reverse* disease will be of paramount importance to HGPS patients who already suffer from advanced

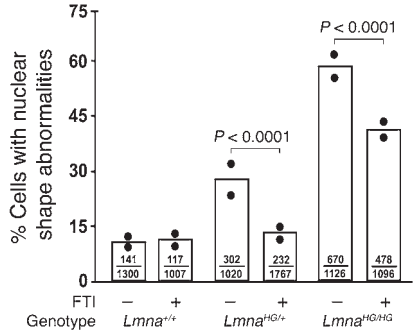

Figure 4
More severe nuclear blebbing in *Lmna*$^{HG/HG}$ embryonic fibroblasts than in *Lmna*$^{HG/+}$ and *Lmna*$^{+/+}$ fibroblasts. The frequency of nuclear blebs in *Lmna*$^{HG/HG}$ embryonic fibroblasts, compared with *Lmna*$^{HG/+}$ and *Lmna*$^{+/+}$ fibroblasts, was significantly increased ($P < 0.0001$ for both comparisons). Treatment of cells with an FTI (2.5 μM ABT-100) reduced the frequency of misshapen nuclei ($P < 0.0001$). Black circles in each bar indicate the results obtained with 2 independent cell lines; ratios within each bar represent the number of cells with misshapen nuclei over the total number of cells evaluated.

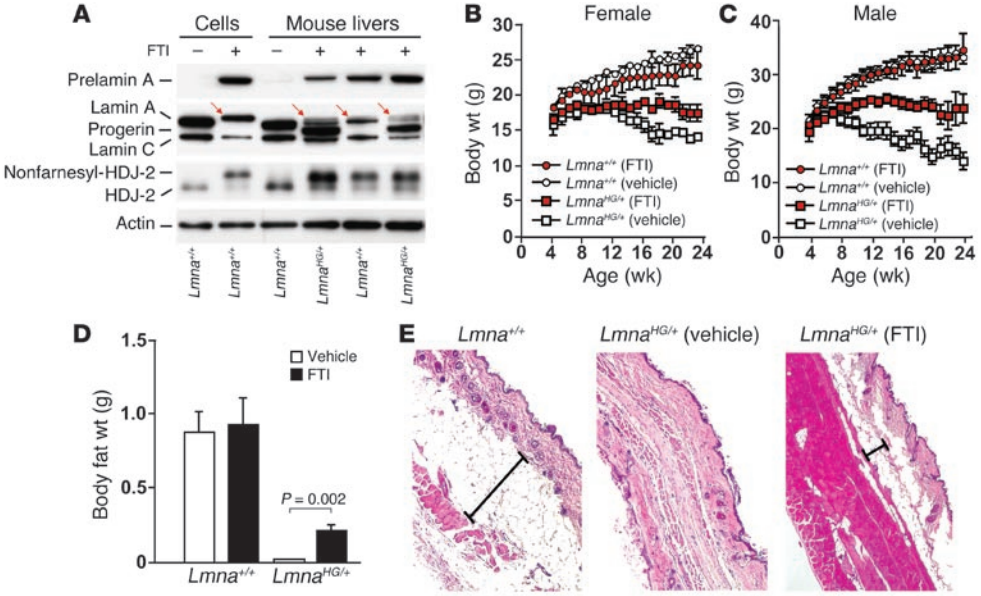

Figure 5
An FTI (ABT-100) ameliorates disease phenotypes in *Lmna*$^{HG/+}$ mice. (**A**) FTI treatment in *Lmna*$^{HG/+}$ and *Lmna*$^{+/+}$ mice leads to the appearance of wild-type prelamin A (with antibodies against prelamin A and lamin A/C) and the appearance of nonfarnesylated HDJ-2 (with an antibody against HDJ-2; nonfarnesyl–HDJ-2) in liver extracts of FTI-treated mice. Red arrows indicate prelamin A, which migrates slightly above mature lamin A. (**B** and **C**) Effect of FTI treatment on body weight in female (**B**) and male (**C**) mice. *Lmna*$^{+/+}$ (circles) and *Lmna*$^{HG/+}$ (squares) mice were given the FTI (red symbols) or vehicle alone (open symbols), beginning at 4 weeks of age, and body weights were measured weekly. Body weight curves for the FTI-treated *Lmna*$^{HG/+}$ mice were significantly improved, compared with those for vehicle-treated *Lmna*$^{HG/+}$ mice ($P < 0.0001$ for both males and females). Male *Lmna*$^{HG/+}$ mice on vehicle, $n = 9$; male *Lmna*$^{HG/+}$ mice on FTI, $n = 7$; female *Lmna*$^{HG/+}$ mice on vehicle, $n = 5$; female *Lmna*$^{HG/+}$ mice on FTI, $n = 10$; male *Lmna*$^{+/+}$ mice on vehicle, $n = 5$; male *Lmna*$^{+/+}$ mice on FTI, $n = 5$; female *Lmna*$^{+/+}$ mice on vehicle, $n = 9$; female *Lmna*$^{+/+}$ mice on FTI, $n = 4$. (**D**) Body fat weights in *Lmna*$^{HG/+}$ mice on FTI or on the vehicle alone. The weight of body fat in *Lmna*$^{HG/+}$ mice was significantly lower than in *Lmna*$^{+/+}$ mice ($P < 0.0001$) and was significantly increased after FTI treatment ($P = 0.002$). (**E**) Representative H&E-stained sections of skin from 6-month-old *Lmna*$^{+/+}$, vehicle-treated *Lmna*$^{HG/+}$, and FTI-treated *Lmna*$^{HG/+}$ mice; $n = 4$ mice in each group examined. The black line spans the layer of subcutaneous fat.

disease. Another key issue for future studies will be to determine whether nonfarnesylated progerin (which is present during FTI treatment) has the potential to elicit disease phenotypes over the long term.

Methods

A gene-targeted model of HGPS. Previously, we generated chimeric mice from mouse embryonic stem cells with a mutant *Lmna* allele (*Lmna*^{HG}) yielding exclusively progerin and bred those mice to generate *Lmna*$^{HG/+}$ embryonic fibroblasts (9). In the current study, we bred *Lmna*$^{HG/+}$ mice to obtain *Lmna*$^{HG/HG}$ mice. Genotyping was performed by PCR with genomic DNA from tail biopsies (9). All mice had a mixed genetic background (~75% C57BL/6 and ~25% 129/OlaHsd). The mice were fed a chow diet and housed in a virus-free barrier facility with a 12-hour light/12-hour dark cycle. Body weights and the ability to hang upside down from a grid (14) were assessed weekly. UCLA's Animal Research Committee approved all procedures.

An FTI, ABT-100 (17), was mixed in drinking water containing 0.4% hydroxy propyl methyl cellulose and 1.0% ethanol at a concentration of 0.3 mg/ml, so as to deliver a dose of approximately 39 mg/kg/d. The vehicle control consisted of drinking water with 0.4% hydroxy propyl methyl cellulose and 1.0% ethanol. Blood samples were collected between 4:00 and 5:30 am; the mean concentration of ABT-100 in the plasma of *Lmna*$^{HG/+}$ mice ($n = 5$) was 0.7104 μg/ml. The treatments were continued until 6 months of age; at that point, surviving mice were euthanized.

Tomographic analyses. *Lmna*$^{+/+}$, *Lmna*$^{HG/+}$, and *Lmna*$^{HG/HG}$ mice were examined by compact cone-beam tomography (μCT 40 scanner; Scanco Medical). Whole-body scans were performed in the axial plane mounted in a cylindrical sample holder at medium resolution with a current of 0.16 mA and a voltage of 70 kilovolt peak (kVp), at an isotropic voxel size of 20.5 μm for the skulls and 30.7 μm for the remainder of the skeleton.

Cortical thickness and degree of mineralization of the cortical bone in the proximal portion of the posterior ninth left rib were determined by μCT scanning; the X-ray tube operated at 55 kVp and 145 μA. Scans of transverse sections of the rib were obtained at 10-μm nominal resolution (high-resolution mode). Two-dimensional images were reconstructed in 2,048 × 2,048–pixel matrices using a standard convolution back-projection procedure with a Shepp and Logan filter, and a cortical volume of interest (VOI) was defined for each measurement. A constrained 3-dimensional Gaussian filter was used to suppress noise. The mineralized tissue was segmented with a fixed threshold for all samples. A manufacturer-provided hydroxyapatite phantom of known density was used to calibrate the system, allowing us to estimate the degree of mineralization of the cortical bone tissue.

Standard skeletal X-rays were performed with a Faxitron X-ray system (Faxitron X-ray Corp.) at 30 kV for 2 seconds. The degree of kyphosis of the spine (kyphotic index) was calculated as described previously (23).

Analysis of rib fractures in Lmna$^{HG/+}$ *mice.* *Lmna*$^{+/+}$ and *Lmna*$^{HG/+}$ mice were euthanized at 8, 16, 24, and 28 weeks of age. The interior of the thorax was photographed with a digital camera, and rib fractures were counted.

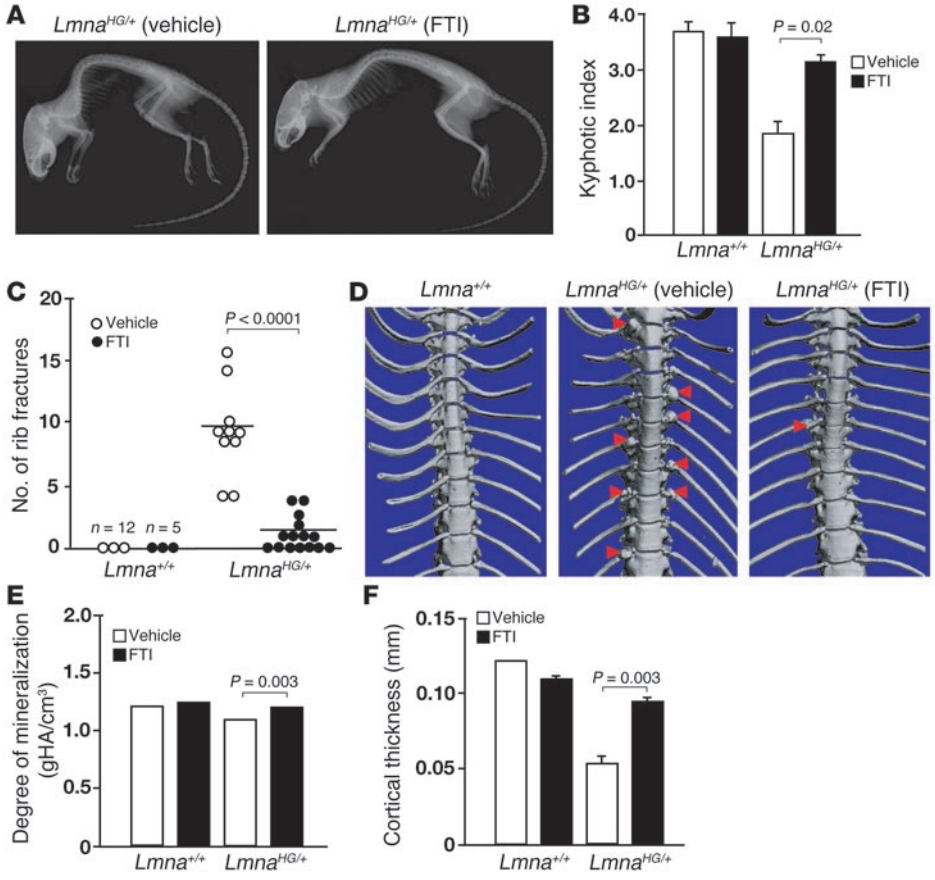

Figure 6
An FTI (ABT-100) ameliorates bone disease in *Lmna*$^{HG/+}$ mice. (**A**) Radiographs of a 6-month-old vehicle-treated *Lmna*$^{HG/+}$ mouse and a littermate FTI-treated *Lmna*$^{HG/+}$ mouse. (**B**) Kyphotic index in FTI-treated and vehicle-treated *Lmna*$^{HG/+}$ and *Lmna*$^{+/+}$ mice. The degree of kyphosis in *Lmna*$^{HG/+}$ mice was greater (a smaller kyphotic index) than in *Lmna*$^{+/+}$ mice ($P < 0.0001$) and was significantly reduced (a larger kyphotic index) after FTI treatment ($P = 0.02$; $n = 10$ per group). (**C**) Reduced number of rib fractures in FTI-treated *Lmna*$^{HG/+}$ mice. After 24 weeks, surviving mice were euthanized, and the number of rib fractures was counted. The number of rib fractures in the FTI-treated *Lmna*$^{HG/+}$ mice was significantly lower than in vehicle-treated *Lmna*$^{HG/+}$ mice ($P < 0.0001$). (**D**) μCT scans illustrating reduced numbers of rib fractures in FTI-treated *Lmna*$^{HG/+}$ mice. Red arrowheads indicate rib fractures and surrounding callus. In the FTI-treated mouse, there was thinning of 1 rib along with a small amount of callus. No rib fractures were observed in *Lmna*$^{+/+}$ mice. (**E** and **F**) FTI treatment improved bone mineralization (**E**) and bone cortical thickness (**F**) in *Lmna*$^{HG/+}$ mice without affecting the bones of *Lmna*$^{+/+}$ mice. Error bars are too small to be seen in **E**. gHA/cm^3, grams of hydroxyapatite per cubic centimeter.

Body fat measurements. *Lmna*$^{+/+}$ and *Lmna*$^{HG/+}$ mice were euthanized at 8, 16, 24, and 28 weeks of age. The major fat pads (reproductive, inguinal, and mesenteric) were isolated and weighed.

Histology. Tissues were fixed in 10% formalin for 24 hours and dehydrated in 50% ethanol. The tissues were then embedded in paraffin, and 5-μm sections were stained with H&E.

Treatment of cells with the FTI and Western blots. Adherent early-passage mouse embryonic fibroblasts in 6-well tissue culture plates were incubated with the vehicle control (DMSO) or 2.5 μM ABT-100 in culture medium at 37°C for 48 hours. The cells were washed with PBS, and urea-soluble extracts were prepared (24). Liver and aorta samples were collected and frozen in liquid nitrogen, and urea-soluble extracts were prepared and analyzed by SDS-PAGE and Western blotting (15). The antibody dilutions were 1:6,000 for a rabbit anti-prelamin A antiserum, 1:400 for a goat anti-lamin A/C antibody (Santa Cruz Biotechnology Inc.), 1:500 for a mouse anti–HDJ-2 antibody (NeoMarkers), 1:2,000 for a goat anti-actin IgG (Santa Cruz Biotechnology Inc.), 1:6,000 for HRP-labeled anti-goat IgG (Amersham Biosciences), 1:6,000 for HRP-labeled anti-mouse IgG (Amersham Biosciences). Antibody binding was detected with the ECL Plus chemiluminescence system (Amersham Biosciences) and exposure to x-ray film.

Immunofluorescence microscopy. The percentage of *Lmna*$^{+/+}$, *Lmna*$^{HG/+}$, and *Lmna*$^{HG/HG}$ fibroblasts with misshapen nuclei was assessed by immunofluorescence microscopy. Fibroblasts were grown on coverslips, fixed in 3% paraformaldehyde, permeabilized with 0.2% Triton X-100, and blocked with PBS containing 10% fetal bovine serum and 0.2% bovine serum albumin (15). Cells were incubated for 60 minutes with antibodies against lamin B1 and B2 (sc-6217, 1:400; Santa Cruz Biotechnology Inc.) or lamin A (sc-20680, 1:200; Santa Cruz Biotechnology Inc.). After washing, cells were stained with species-specific Cy3-conjugated secondary antibodies (Jackson ImmunoResearch Laboratories Inc.) and DAPI to visualize DNA. Images were obtained on an Axiovert 40 CFL microscope (Zeiss) with a 63×/1.25 oil immersion objective and processed with AxioVision 4.2 software (Zeiss). Two independent observers blinded to genotype scored nuclear shape abnormalities.

Statistics. Body weight curves were compared with repeated-measures ANOVA and the log-rank test. The degree of mineralization, cortical thickness, number of rib fractures, fat pad weight, and kyphotic index measurements were compared with the 2-tailed Student's *t* test. Data are shown as mean ± SEM. Differences in the percentages of misshapen nuclei were assessed by the χ^2 test.

Acknowledgments
We thank Ken Jarvis for measurements of ABT-100. This work was supported by NIH grants AR050200 and HL76839 and grants from the Progeria Research Foundation. S.H. Yang was supported by a postdoctoral fellowship grant from the American Heart Association, Western States Affiliate.

Received for publication May 2, 2006, and accepted in revised form May 23, 2006.

Address correspondence to: Loren G. Fong or Stephen G. Young, 650 Charles East Young Drive South, Los Angeles, California 90095, USA. Phone: (310) 825-4934; Fax: (310) 206-0865; E-mail: lfong@mednet.ucla.edu (L.G. Fong) or sgyoung@mednet.ucla.edu (S.G. Young).

1. Debusk, F.L. 1972. The Hutchinson-Gilford progeria syndrome. *J. Pediatr.* **80**:697–724.
2. Eriksson, M., et al. 2003. Recurrent *de novo* point mutations in lamin A cause Hutchinson-Gilford progeria syndrome. *Nature.* **423**:293–298.
3. Ackerman, J., and Gilbert-Barness, E. 2002. Hutchinson-Gilford progeria syndrome: a pathologic study. *Pediatr. Pathol. Mol. Med.* **21**:1–13.
4. Stehbens, W.E., Delahunt, B., Shozawa, T., and Gilbert-Barness, E. 2001. Smooth muscle cell depletion and collagen types in progeric arteries. *Cardiovasc. Pathol.* **10**:133–136.
5. Stehbens, W.E., Wakefield, S.J., Gilbert-Barness, E., Olson, R.E., and Ackerman, J. 1999. Histological and ultrastructural features of atherosclerosis in progeria. *Cardiovasc. Pathol.* **8**:29–39.
6. Young, S.G., Fong, L.G., and Michaelis, S. 2005. Prelamin A, Zmpste24, misshapen cell nuclei, and progeria — new evidence suggesting that protein farnesylation could be important for disease pathogenesis. *J. Lipid Res.* **46**:2531–2558.
7. Goldman, R.D., et al. 2004. Accumulation of mutant lamin A causes progressive changes in nuclear architecture in Hutchinson-Gilford progeria syndrome. *Proc. Natl. Acad. Sci. U. S. A.* **101**:8963–8968.
8. Scaffidi, P., and Misteli, T. 2005. Reversal of the cellular phenotype in the premature aging disease Hutchinson-Gilford progeria syndrome. *Nat. Med.* **11**:440–445.
9. Yang, S.H., et al. 2005. Blocking protein farnesyltransferase improves nuclear blebbing in mouse fibroblasts with a targeted Hutchinson-Gilford progeria syndrome mutation. *Proc. Natl. Acad. Sci. U. S. A.* **102**:10291–10296.
10. Toth, J.I., et al. 2005. Blocking protein farnesyltransferase improves nuclear shape in fibroblasts from humans with progeroid syndromes. *Proc. Natl. Acad. Sci. U. S. A.* **102**:12873–12878.
11. Mallampalli, M.P., Huyer, G., Bendale, P., Gelb, M.H., and Michaelis, S. 2005. Inhibiting farnesylation reverses the nuclear morphology defect in a HeLa cell model for Hutchinson-Gilford progeria syndrome. *Proc. Natl. Acad. Sci. U. S. A.* **102**:14416–14421.
12. Capell, B.C., et al. 2005. Inhibiting farnesylation of progerin prevents the characteristic nuclear blebbing of Hutchinson-Gilford progeria syndrome. *Proc. Natl. Acad. Sci. U. S. A.* **102**:12879–12884.
13. Glynn, M.W., and Glover, T.W. 2005. Incomplete processing of mutant lamin A in Hutchinson-Gilford progeria leads to nuclear abnormalities, which are reversed by farnesyltransferase inhibition. *Hum. Mol. Genet.* **14**:2959–2969.
14. Bergo, M.O., et al. 2002. *Zmpste24* deficiency in mice causes spontaneous bone fractures, muscle weakness, and a prelamin A processing defect. *Proc. Natl. Acad. Sci. U. S. A.* **99**:13049–13054.
15. Fong, L.G., et al. 2004. Heterozygosity for Lmna deficiency eliminates the progeria-like phenotypes in Zmpste24-deficient mice. *Proc. Natl. Acad. Sci. U. S. A.* **101**:18111–18116.
16. Sullivan, T., et al. 1999. Loss of A-type lamin expression compromises nuclear envelope integrity leading to muscular dystrophy. *J. Cell Biol.* **147**:913–919.
17. Ferguson, D., et al. 2005. Antitumor activity of orally bioavailable farnesyltransferase inhibitor, ABT-100, is mediated by antiproliferative, proapoptotic, and antiangiogenic effects in xenograft models. *Clin. Cancer Res.* **11**:3045–3054.
18. Fong, L.G., et al. 2006. A protein farnesyltransferase inhibitor ameliorates disease in a mouse model of progeria. *Science.* **311**:1621–1623.
19. Mounkes, L.C., Kozlov, S., Hernandez, L., Sullivan, T., and Stewart, C.L. 2003. A progeroid syndrome in mice is caused by defects in A-type lamins. *Nature.* **423**:298–301.
20. Mounkes, L.C., Kozlov, S.V., Rottman, J.N., and Stewart, C.L. 2005. Expression of an LMNA-N195K variant of A-type lamins results in cardiac conduction defects and death in mice. *Hum. Mol. Genet.* **14**:2167–2180.
21. Arimura, T., et al. 2005. Mouse model carrying H222P-Lmna mutation develops muscular dystrophy and dilated cardiomyopathy similar to human striated muscle laminopathies. *Hum. Mol. Genet.* **14**:155–169.
22. Varga, R., et al. 2006. Progressive vascular smooth muscle cell defects in a mouse model of Hutchinson-Gilford progeria syndrome. *Proc. Natl. Acad. Sci. U. S. A.* **103**:3250–3255.
23. Laws, N., and Hoey, A. 2004. Progression of kyphosis in mdx mice. *J. Appl. Physiol.* **97**:1970–1977.
24. Steinert, P., Zackroff, R., Aynardi-Whitman, M., and Goldman, R.D. 1982. Isolation and characterization of intermediate filaments. *Methods Cell Biol.* **24**:399–419.